International Journal of
MATERIALS RESEARCH

Zeitschrift für METALLKUNDE

Original Contributions

Piotr Łakoma[a], André Ditze[b], Christiane Scharf[c]
[a] Clausthal University of Technology, Institute of Metallurgy, Clausthal-Zellerfeld, Germany
[b] Engineering Office MetuRec, Clausthal-Zellerfeld, Germany
[c] Helmholtz Centre Dresden Rossendorf, Helmholtz Institute Freiberg for Resource Technology, Freiberg, Germany

Dendritic structure formation of magnesium alloys for the manipulation of corrosion properties: Part 1 – microstructure

Besides impurities in magnesium alloys containing aluminum, the microstructure also plays a role in the corrosion properties of the alloy. By targeted manipulation of grain size, secondary dendrite arm spacings and segregation in terms of amount and position, the corrosion properties are expected to be improved. For this, experiments were carried out by casting alloys with 0, 3, 6, 9, and 12 % aluminum into a mold with different applied cooling rates. The samples were analyzed regarding microstructure and composition, and the grain size and secondary dendrite arm spacings, as a function of aluminum content and cooling rate, were modeled. The results show a decrease in grain size and secondary dendrite arm spacings with an increased cooling rate. The segregated β phase was predominantly situated at the grain boundaries as divorced eutectic and in lamellar form. The assumed influences on the corrosion properties will be examined in Part 2.

Keywords: Magnesium alloy; Microstructure; Corrosion behavior; SDAS

1. Introduction

Due to the very ignoble character of magnesium alloys they are threatened by corrosion when electrolytes (humidity, road salt, etc.) are present. This can lead to failure in parts that are made of magnesium alloys. By using magnesium alloys that have an extremely low amount of impurities, corrosion resistance can be achieved that also enables magnesium alloys to be used for external use, such as in the transport sector.

1.1. Relations between microstructure and corrosion properties

During the solidification process of magnesium alloys containing aluminum, micro galvanic cells are formed through the formation of the β phase ($Mg_{17}Al_{12}$). The β phase shows a more positive electrochemical potential than the primarily formed α phase. Depending on the cooling rate, the structure changes with respect to grain size, dendrite formation and proportion of the β phase. Kind and number of micro galvanic cells and electrochemical potential differences between them are also changing. The principle of microgalvanic corrosion of magnesium alloys is shown in Fig. 1 [1]. Hence, the aim was to examine the relation between the microstructure and the corrosion resistance of magnesium and magnesium alloys containing aluminum. By experimentally adjusting grain size and secondary dendrite arm spacings (*SDAS*) through a targeted and defined cooling process with subsequent examination – by immersion and salt spray test – of the corrosion of the samples, we expected to establish a relation between the structure and corrosion behavior of the magnesium alloys and show possibilities where corrosion resistance could be improved.

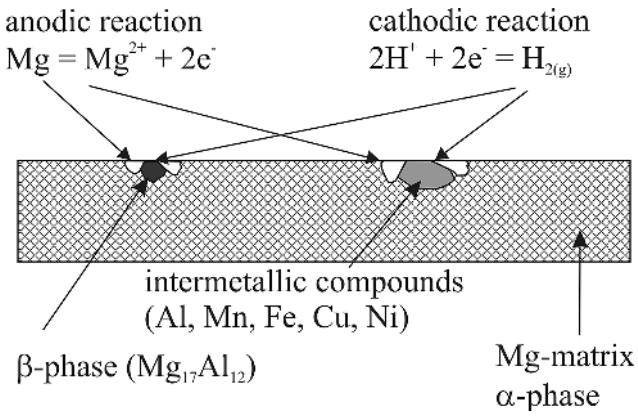

Fig. 1. Microgalvanic corrosion of magnesium alloy, Ref. [1].

Numerous publications have reported on the importance of magnesium alloy structures with respect to corrosion properties Refs. [2–28]. However, a correlation between *SDAS* in the microstructure and corrosion properties has not been examined. Some authors Song et al. [29] have found a relation between tensile strength and corrosion rate of the die casting alloy AZ91D. Other authors Refs. [28, 30] have determined the influence of grain size with pure magnesium on corrosion. They came to the conclusion that the formation of grain structure is of particular importance. Together with the result from Refs. [28, 29, 31–35], the conclusion seems to be that *SDAS* plays an important role in strength and corrosion properties. Because of composition differences and the formation of dendrite arms, as well as the concentration distribution in the structure, a relation to corrosion properties was expected.

1.2. Modeling of microstructure and corrosion behavior

The formation of the 3-dimensional α dendrites and the preferred growth orientations of primary and secondary branches among others of Mg–Zn and Mg–Al alloys were modeled by the authors of Refs. [36–39]. For calculating primary and secondary dendrite arm distances as a function of the solidification conditions, several mathematical models have been described in the literature, Refs. [40–43]. Composition, growth rate, and thermal gradients play important roles, as does material transport through convection and diffusion. The models of Bouchard and Kirkaldy [40] and Kirkwood [41] are often used to describe the *SDAS*. Methods for corrosion investigations are immersion test, salt-spray test and electrochemical tests. The immersion test is preferred for long term investigations. The time dependent corrosion rate can be described by the model of Ditze and Scharf [44]. The modeling of *SDAS* and the time-dependent corrosion is supposed to underpin the experimental results scientifically. Regarding the alloys, Mg–Al alloys with 0, 3, 6, 9, and 12 % Al (all compositions in mass percentage) were examined.

2. Experimental procedure

2.1. Experimental apparatus and materials

To create alloys by casting and targeted cooling, a mold similar to Quaresma et al. [33], as per Fig. 2, was manufactured. One side is a metallic cooling block made of either copper or steel. The other side is made of insulating aluminum oxide plates that were preheated to 250 °C before the experiments. The inserted ceramic plates with a thickness of 15 mm for the Al_2O_3 mold were from Friatec AG, Germany (Degussit AL 25). The plates and the crucible were coated with boron nitride (BN) before the experiments took place. The BN was used as a suspension (EKamold WS from ESK Ceramics GmbH & Co. KG, Germany) and as a spray (HeBoCoat 401E from Henze Boron Nitride Products GmbH, Germany). The magnesium alloys were produced in a crucible made of steel (∅ 81 × 160 mm). Sulfur hexafluoride 3.0 was used as the protective gas during melting of the alloys and as the flushing gas for the removal of hydrogen Argon 4.6 was used as well as a mixture of 99.5 vol.% Ar 6.0 and 0.5 vol.% Cl_2 5.0 from Linde AG, Germany.

2.2. Execution and evaluation of experiments

To ensure reproducibility of the results, three experiments for each test series were performed. The samples for the metallographic and corrosion examinations demanded a defined microstructure. Accordingly, two samples were cast without thermocouples at the location of the metal. The third mold was used for thermal analysis and recording of solidification. For this, thermocouples that record cooling curves via a data logger were embedded with a defined distance from the cooling block. The alloys were cast with an overheating of 11 % regarding the respective liquidus temperature. After the cooling process, the samples were cut out of the cast metal block at positions having had different cooling rates. The sample ranges A, B, and C for the metallographic examinations are differently shaded in Fig. 2. The lengths are 18, 20, and 10 mm, respectively. Because the corrosion of magnesium is determined particularly by the content of Cu, Ni, and Fe, only impurity contents of 6 ppm Cu, up to 6 ppm Ni, 10 ppm Mn, and 5 ppm Fe were selected for the samples cast with 0, 3, 6, 9, and 12 % aluminum content. The compositions were determined by a wet-chemical ICP-OES (inductively coupled plasma-optical emission spectroscopy) analysis after sampling. Determination of the cooling rates at the locations of the thermocouples took place directly from the recorded cooling curves. For that, the first derivative of the cooling curve was taken and the inflection point of the cooling curve below the liquidus temperature was determined. The tangent dT/dt shows the cooling rate (*CR*) of the alloy. For the metallographic examinations, the samples were prepared in the usual form and examined by light microscopy and SEM-EDX (scanning electron microscopy with energy dispersive X-ray spectroscopy) with regard to grain size, *SDAS*, phase fractions, the composition of phases through a point, line and area analysis. An example of an *SDAS* determination for Mg–Al alloys can be seen in Fig. 3.

2.3. Validation of the experimental set-up on the basis of literature

A lot of investigations regarding *SDAS* and varying cooling rates were carried out with aluminum alloys containing copper. To prove the experimental adaption to the summarized literature data in Bouchard and Kirkaldy [34], samples

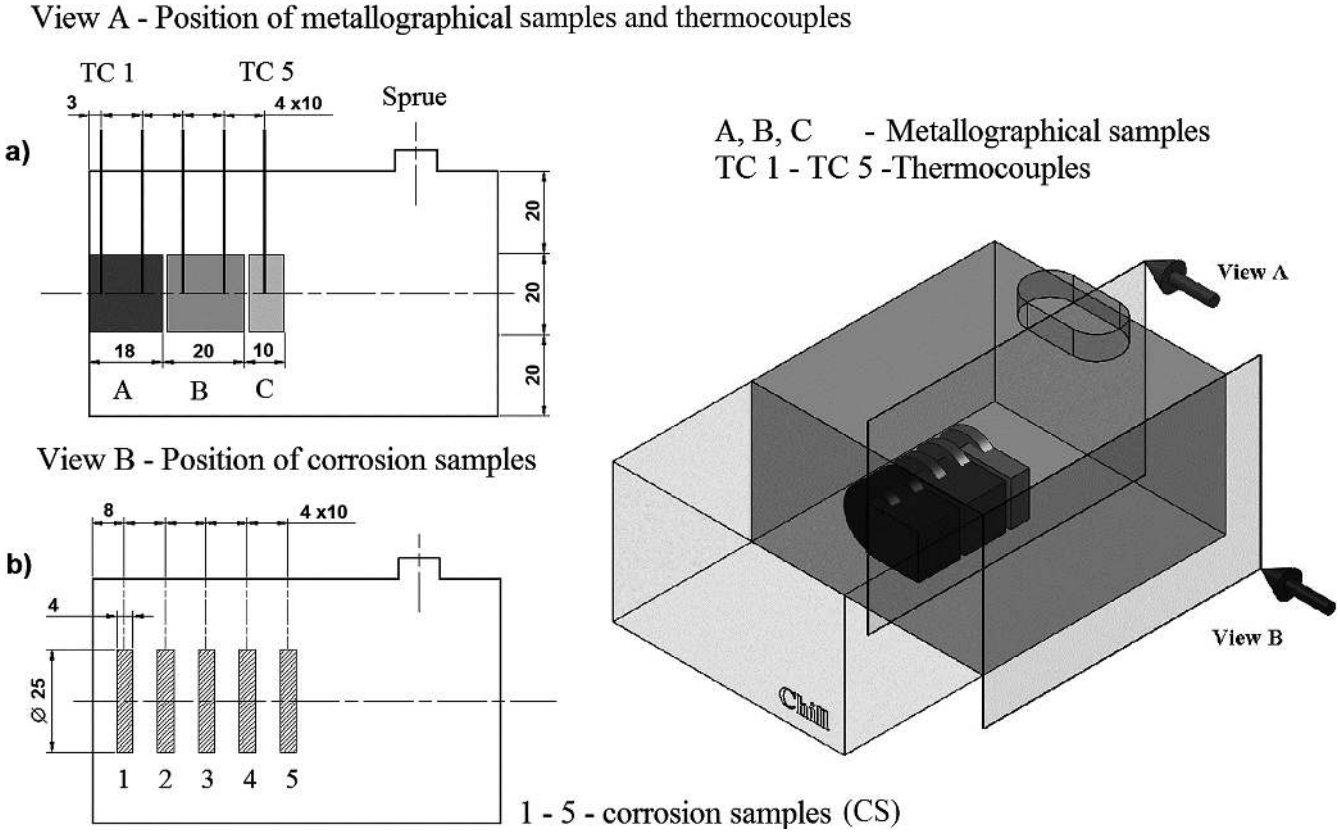

Fig. 2. Mold used to manufacture the magnesium alloy samples under defined cooling conditions. Dimensions in mm. Due to the cutting tool, there is a gap of 2 mm between A, B, and C.

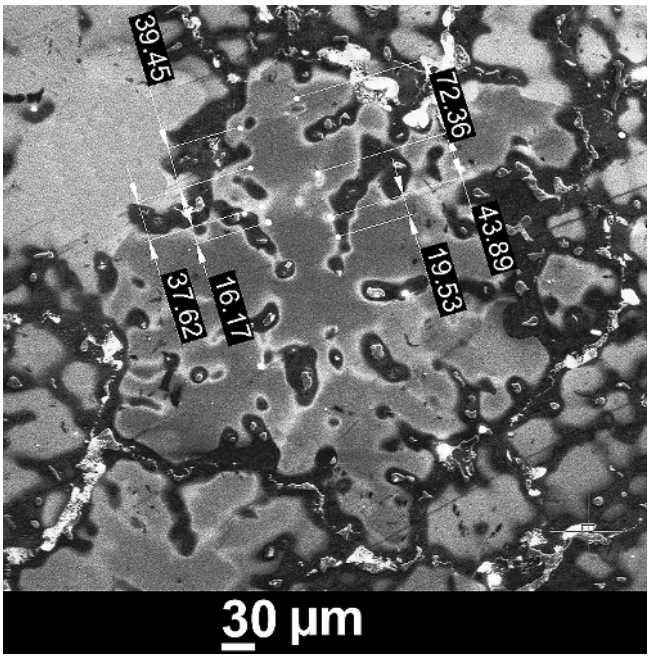

Fig. 3. Example of an *SDAS* determination of an Mg–Al alloy with 12 % Al (11.9 % Al, 2 ppm Cu, 6 ppm Fe, and 2 ppm Ni). Measurement point: 48 mm from the cooling block.

from Al-4.5 %Cu and Al-4.75 %Cu were prepared. The determined cooling rates were then attributed to the drawn distances of the cooling unit in Fig. 2. The results of the *SDAS* measurements for the examined aluminum–copper alloys [45–51] are compared in Fig. 4 with those from Bouchard and Kirkaldy [40]. The results from the used mold have good conformity with the results in the literature. A connection to the literature data is therefore assured.

3. Microstructure of magnesium-aluminum alloys

For the examined aluminum contents of up to 12 %, both α and β phases ($Mg_{17}Al_{12}$) occur in the structure. At first, the α phase separates during the solidification process forming 3-dimensional dendrites with primary and secondary branches as illustrated and modeled in Refs. [36–39]. Because of the slow diffusion in the solid state, the melt, depending on the aluminum content and cooling rate, can enrich with aluminum to a point where the residual melt solidifies eutectically. Hereby, the α proportion of the eutectic crystallizes partially to the primarily separated α phase so that a solid β phase remains. The eutectic has degenerated. The α phase, supersaturated with aluminum, can separate the β phase during cooling as well.

3.1. Influence of aluminum content on phase fractions and composition

Figure 5 shows the SEM picture of an alloy with 3 % Al and a line scan through the structure. The structure consists mainly of the α phase with very little β phase. Corresponding to the Mg–Al only phase diagram a small eutectic proportion is expected even with actual solidification. The line

scan shows the lowest Al content (around 3 %) in the middle of the dendrites. This is significantly higher than what can be expected with around 1 % for the primary crystallization. However, the middle of a dendrite in the 2D picture is not explicitly defined as dendrites are three-dimensional. Still, the increasing content of aluminum towards the grain boundaries is clearly recognizable. For an alloy with 9 % aluminum, an aluminum content of 6.9 % (point 1) was measured in the middle of the dendrite in Fig. 6. This is also higher than the expected aluminum content of the first crystallizing α of around 3 %. The aluminum content increases to 8.2 % at the edge of the dendrite (point 5). The β phase of the divorced eutectic is situated at the grain boundary and in the interdendritic areas. However, the measured aluminum content at point 2 of around 28 % is significantly below the content of the β phase (42 % Al), because α is also measured. Both measurement points 3 and 4 have 11 % aluminum and, therefore, are around the maximum aluminum content of 12.5 % Al of the α phase at the eutectic temperature. This is reached in the lamellar area of point 6. An analytic separation of the lamellar area in α and β was no longer possible. However, α is predominantly measured. The area scan demonstrates how aluminum is spread across the structure. The center of the α dendrites is enclosed by a continuously increasing aluminum content area. This is followed by eutectic and solid β phase from the divorced eu-

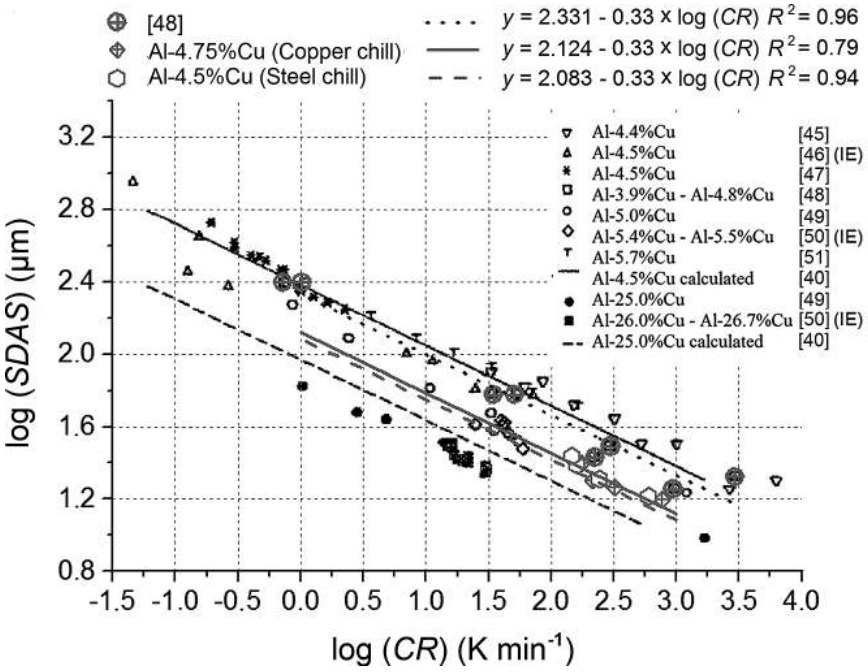

Fig. 4. *SDAS* as a function of the cooling rate (*CR*) for Al–Cu alloys according to Bouchard and Kirkaldy [40]. Gray squares and hexagons are own results. IE = unsteady solidification.

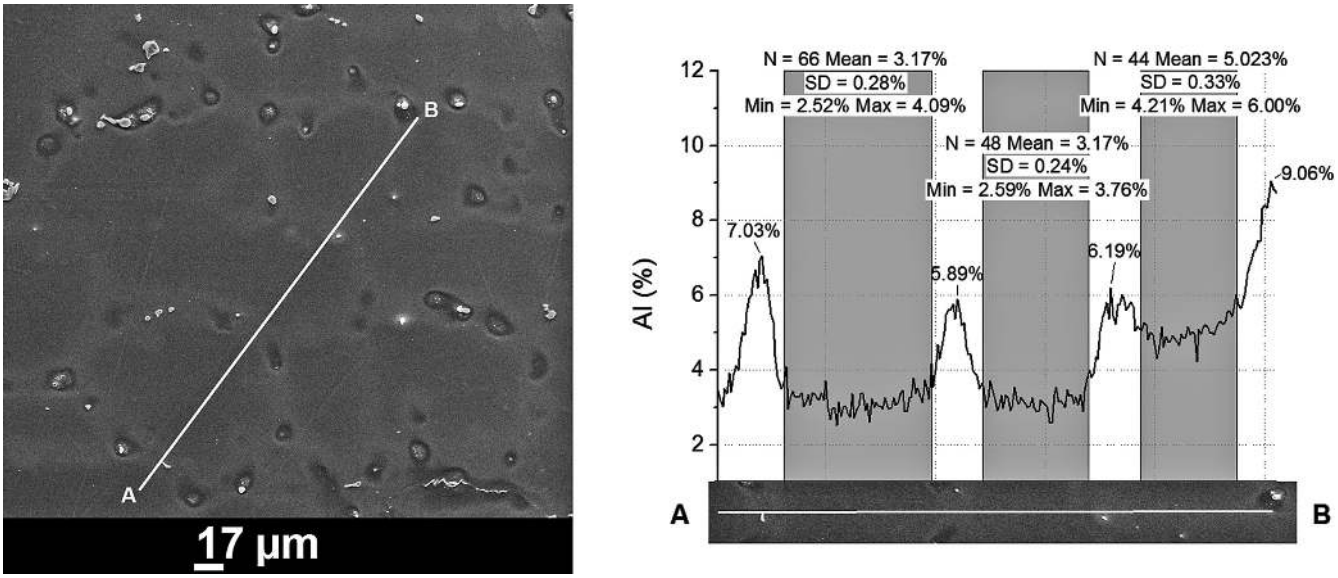

Fig. 5. BSE (backscattered electron) image of a Mg-3 %Al alloy (2.88 % Al, 5 ppm Cu, 21 ppm Fe, and <1 ppm Ni) at a distance of 48 mm from the cooling area and a cooling rate of 2.26 K s^{-1} (left). Line scan with respect to Al content (right).

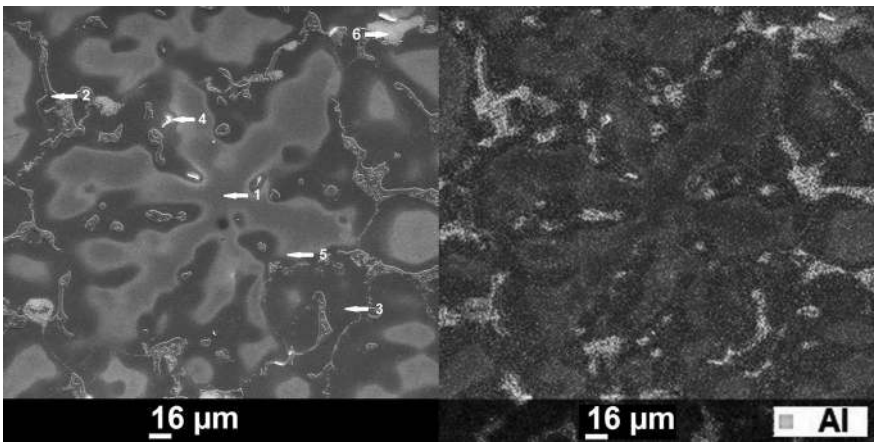

Fig. 6. BSE (backscattered electron) image of a Mg-9 %Al alloy (9.05 % Al, 10 ppm Cu, 50 ppm Fe, and 4 ppm Ni) at a distance of 44 mm from the cooling area and a cooling rate of 2.32 K s^{-1} with marked measurement points (left). Area scan with respect to Al content (right).

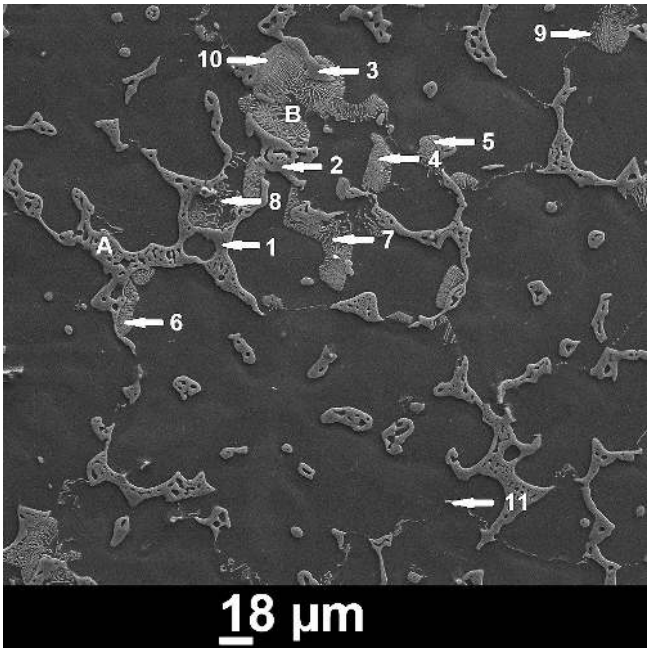

Fig. 7. SE (secondary electron) image of a Mg-12 %Al alloy (12.3 % Al, 6 ppm Cu, 33 ppm Fe, and 1 ppm Ni) at a distance of 14 mm from the cooling area and a cooling rate of 5.04 K s^{-1} with marked measurement points.

tectic. The structure of a magnesium alloy with 12 % Al is shown in Fig. 7. With almost the same enlargement as shown in Fig. 6, the smaller grain size and the considerably larger proportion of β phase can be recognized. The measurement points 1, 2, and 3 account for 35 % Al on average, which approximately corresponds to the eutectic composition (33.5 % Al). The lamellar formation (points 4 – 10) has 13 % Al on average. The lamellar areas, shown in Fig. 8, are enlarged. Figure 8 shows that a lot of the α phase is measured in the lamellar area. With an increased aluminum content, the proportion of the β phase from the eutectic and saturated phase increases. The aluminum contents in the primary and secondary dendrites depend on the cooling rates. Rapid cooling of the melt results in aluminum contents in the α phase that are significantly higher than the equilibrium content according to the phase diagram.

3.2. Influence of cooling rate and composition on the microstructure, grain size and *SDAS*

The grain sizes in the structure of the alloys also depend on the cooling rate and the composition. They, in turn, influence the *SDAS*. As a result, the determined microstructure should have a considerable influence on the corrosion properties. Also, the alignment of the grains during different cooling conditions can play a role in the corrosion properties. However, it was shown that the columnar to equiaxed transition (CET) for all alloys have a distance of around 3.5 mm to the cooling block. Thus, the transition is close to the cooling unit. Therefore, the samples have an equiaxed structure. The influence of the aluminum content on the reduction of grain size, as well as the change in the formation of the dendritic structure, is illustratively shown by the SEM image of the broken samples in Fig. 9. Besides the grain size, *SDAS*, and segregations, the alignment of phases in the structure should also be important for corrosion behavior. The divorced eutectic consists of an α phase and a β phase that accumulate predominantly at the grain boundaries. From the micrographs, the dense β phase and the segregated β phase from solid solution can be differentiated. Figure 10 shows both phase proportions. The determination of the area proportions of the dense β phase on the grain boundaries and in the grain, as well as the lamellar β segregations according to the linear intercept method, are shown in Fig. 11. With increased cooling rates, the proportions of lamellar β segregations increase, whereas the proportions of dense β phase remain rather constant. The alloys with 3 and 6 % aluminum both have a small proportion of β phase and the values are uncertain. Aluminum makes the grain finer. However, the cooling rate has the biggest influence on the grain size. The determined grain sizes [51] are shown in comparison to Günther et al. [52] in Fig. 12. The effect of aluminum on the fineness of the grain is small when aluminum content is above 6 %. Significant differences resulting from the aluminum contents can be noticed with respect to grain size only when the aluminum content is 3 %. However, there is a tendency to decrease in grain size for increasing aluminum contents of 6 to 12 %. The fundamental progression of dependency of grain sizes was confirmed by Günther et al. [52] for AZ alloys (A = weight percent aluminum, Z = weight percent zinc). The grain sizes were, however, much lower because these alloys contain additional zinc and manganese. Moreover, silicon carbide was

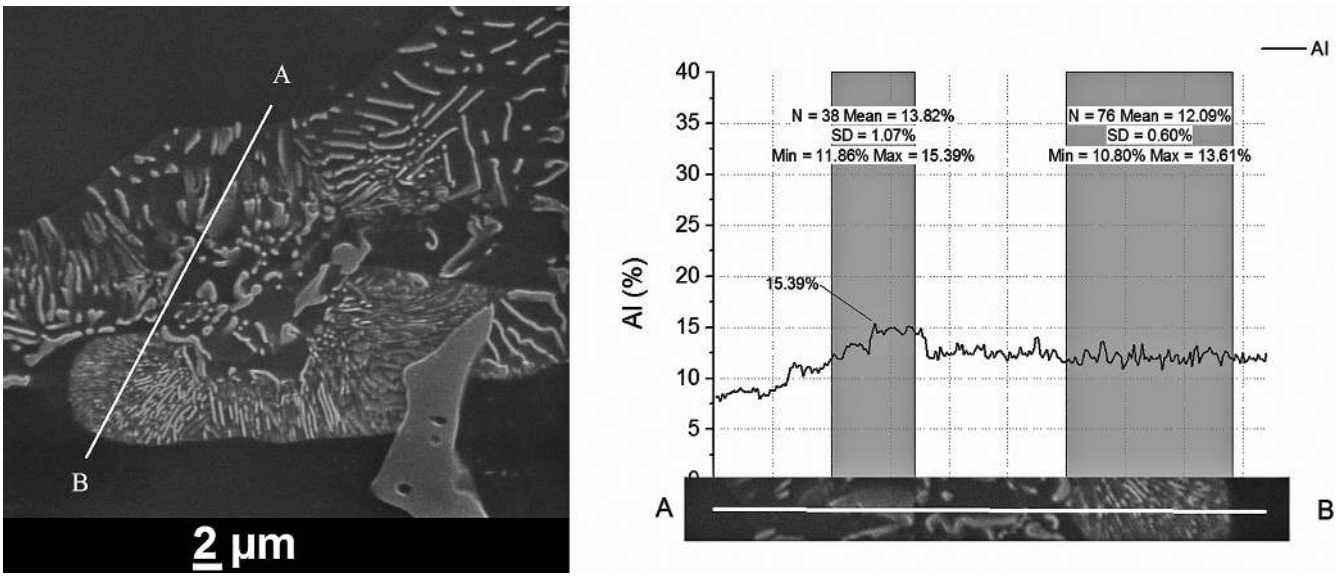

Fig. 8. SE (secondary electron) image of a Mg-12 %Al alloy (12.3 % Al, 6 ppm Cu, 33 ppm Fe, and 1 ppm Ni) at a distance of 8 mm from the cooling area and a cooling rate of 7.68 K s^{-1} (left). Line scan for aluminum along A–B (right).

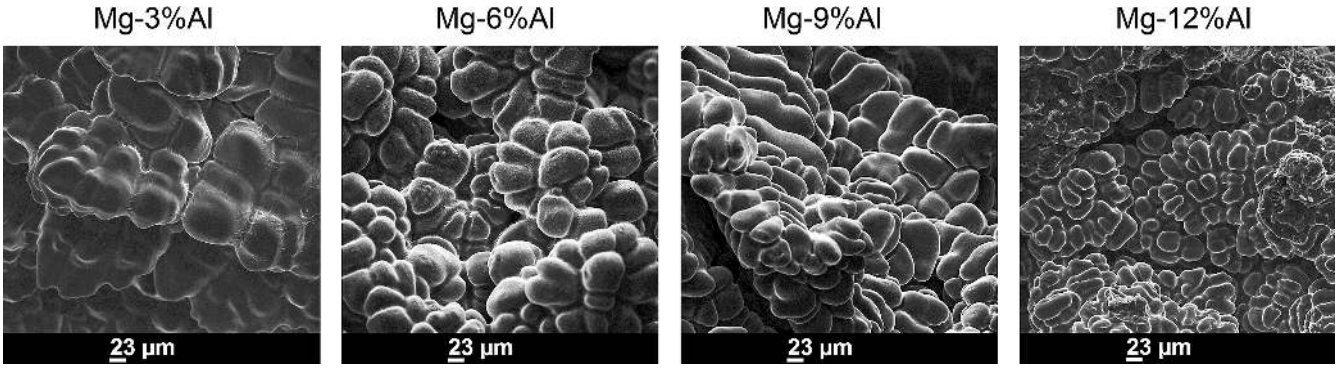

Fig. 9. Influence of aluminum on the form and formation of dendrites at a distance of 48 mm from the cooling block.

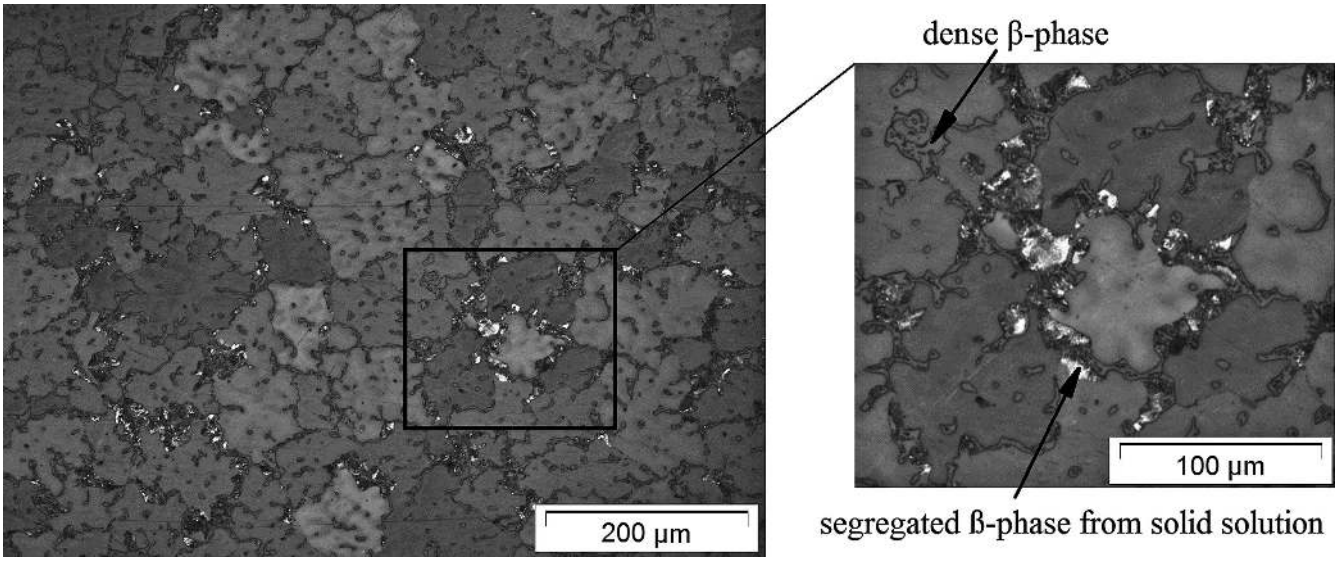

Fig. 10. Solid β phase and separation of the ß phase from the saturated α phase of an alloy with 12 % Al and at a distance of 10 mm from the cooling block (cooling rate 8.9 K s^{-1}).

used for grain refining. With increasing cooling rate, the *SDAS* decreases with a gradient similar to that of the grain sizes, as shown in Fig. 13. Because the *SDAS* has minimal dependence on aluminum content, a balance line for all *SDAS* was drawn into Fig. 13. A comparison of our own results with data from the literature with respect to *SDAS* is shown in Fig. 14 [32, 53–60]. For comparison, lines with gradients of –1/2, –1/3, and –1/5 are drawn in. Despite dispersion of the values they are in accordance with the existing literature because the spread is at least the same way there.

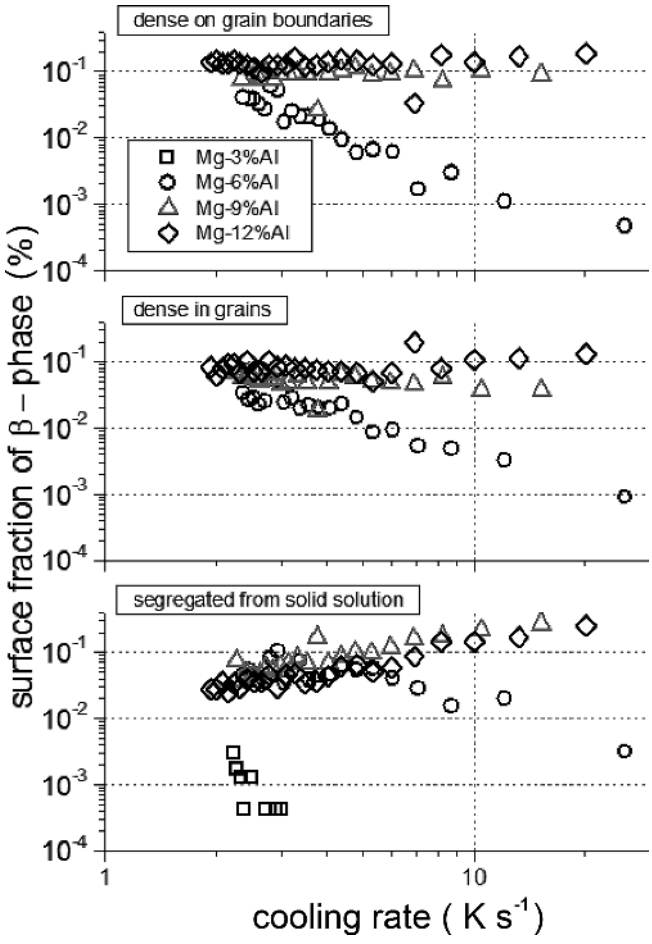

Fig. 11. The area proportion of the dense β phase at the grain boundaries, the dense β phase in the grain, and the lamellar eutectic of the magnesium alloys with 3 to 12 % Al as a function of the cooling rate.

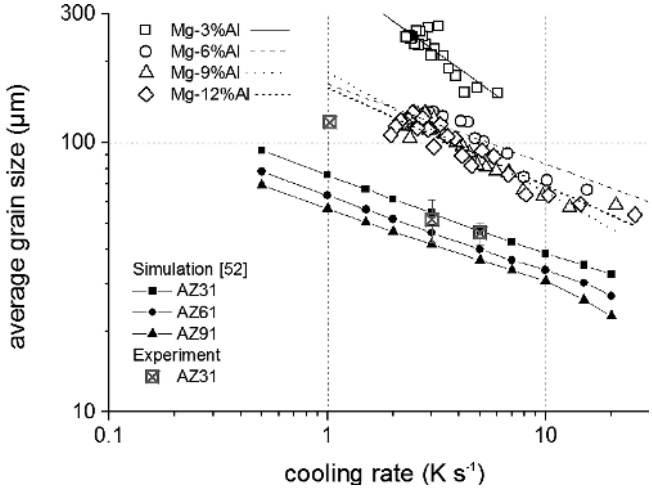

Fig. 12. Grain sizes of magnesium alloys with 3–12 % aluminum as a function of cooling rate.

4. Modeling of grain size and SDAS

For modeling of *SDAS* (λ_2), different approaches are available. Most observe a linear relation of the logarithm of the *SDAS* to the logarithmic cooling rate with a gradient of –1/3, as shown for aluminum alloys in Fig. 4, although the experimental values, determined by the regression, generally lie between 0.3 and 0.4, Ref. [40].

The model of Kirkwood [41] and Kurz and Fischer [42] presents the relation

$$\lambda_2 = K(M \cdot t_{SL})^{1/3} \tag{1}$$

where K is a constant that can be 4.36 according to Ref. [61], 5.04 according to Ref. [41], or 5.50 according to Ref. [42]. The local solidification time t_{SL} in seconds is calculated as a ratio of the solidification range during non-equi-

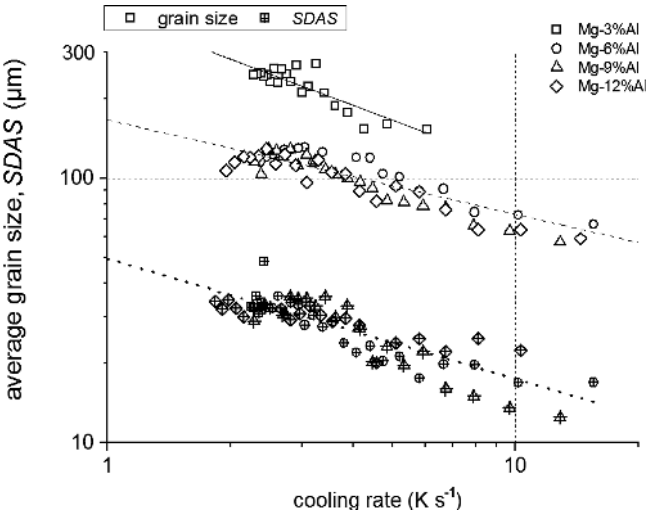

Fig. 13. Grain size and *SDAS* depend on the cooling rate.

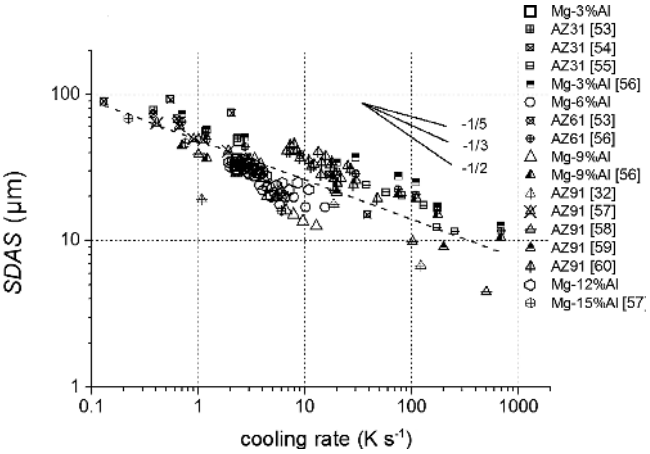

Fig. 14. *SDAS* as a function of the cooling rate. Comparison to literature Refs. [32, 53–60].

librium solidification T_L–T_E (T_L = liquidus temperature, T_E = eutectic temperature = 436 °C) and the cooling rate (CR) in K s^{-1}, Ref. [42]:

$$t_{SL} = \frac{(T_L - T_E)}{CR} \tag{2}$$

$$\lambda_2 = K\left(\frac{M(T_L - T_E)}{CR}\right)^{1/3} \tag{3}$$

with

$$M = -\frac{\Gamma \cdot D}{(1-k)\cdot m_L(C_E - C_0)} \cdot \ln\left(\frac{C_E}{C_0}\right) \tag{4}$$

where Γ is the Gibbs-Thomson coefficient (m · K), D is the diffusion coefficient of the solute (m^2 · s^{-1}), k is the distribution coefficient, m_L is the gradient of liquid line (K/%), C_E is the eutectic concentration 33.5 %, and C_o is the concentration of Al in the alloy (%).

The Gibbs-Thomson coefficient is described by Eq. (5):

$$\Gamma = \frac{\sigma \cdot T_L}{\Delta H_f}(m\,K) \tag{5}$$

where σ is the interfacial energy in a solid-liquid state (J m^{-2}), T_L is the liquidus temperature (K), and ΔH_f is the heat of fusion (J m^{-3}). For the calculation, the thermophysical values according to Table 1 apply [56, 62–64]. Under the use of coefficient M, the related K values can be deter-

Table 1. Thermophysical data for the calculation of coefficients M and K. Data from Refs. [56, 62–64].

Al (%)	$D \times 10^{-9}$ (m^2 s^{-1})	σ (J m^{-2})	$\Delta H_f \times 10^6$ (J m^{-3})	T_L (K)	T_L–T_E (K)	k (–)	$\Gamma \times 10^{-8}$ (K m)	m_L (K/%)	$M \times 10^{-18}$ (m^3 s^{-1})
3	2.99	0.0940	532.2	907.4	198.4	0.321	11.121	–5.228	10.727
6	2.73	0.0475	502.1	892.0	183.0	0.324	5.855	–5.333	4.011
9	2.42	0.0326	476.6	876.3	167.3	0.327	4.127	–5.452	2.129
12	2.05	0.0233	369.0	860.1	151.1	0.331	3.705	–5.557	1.435

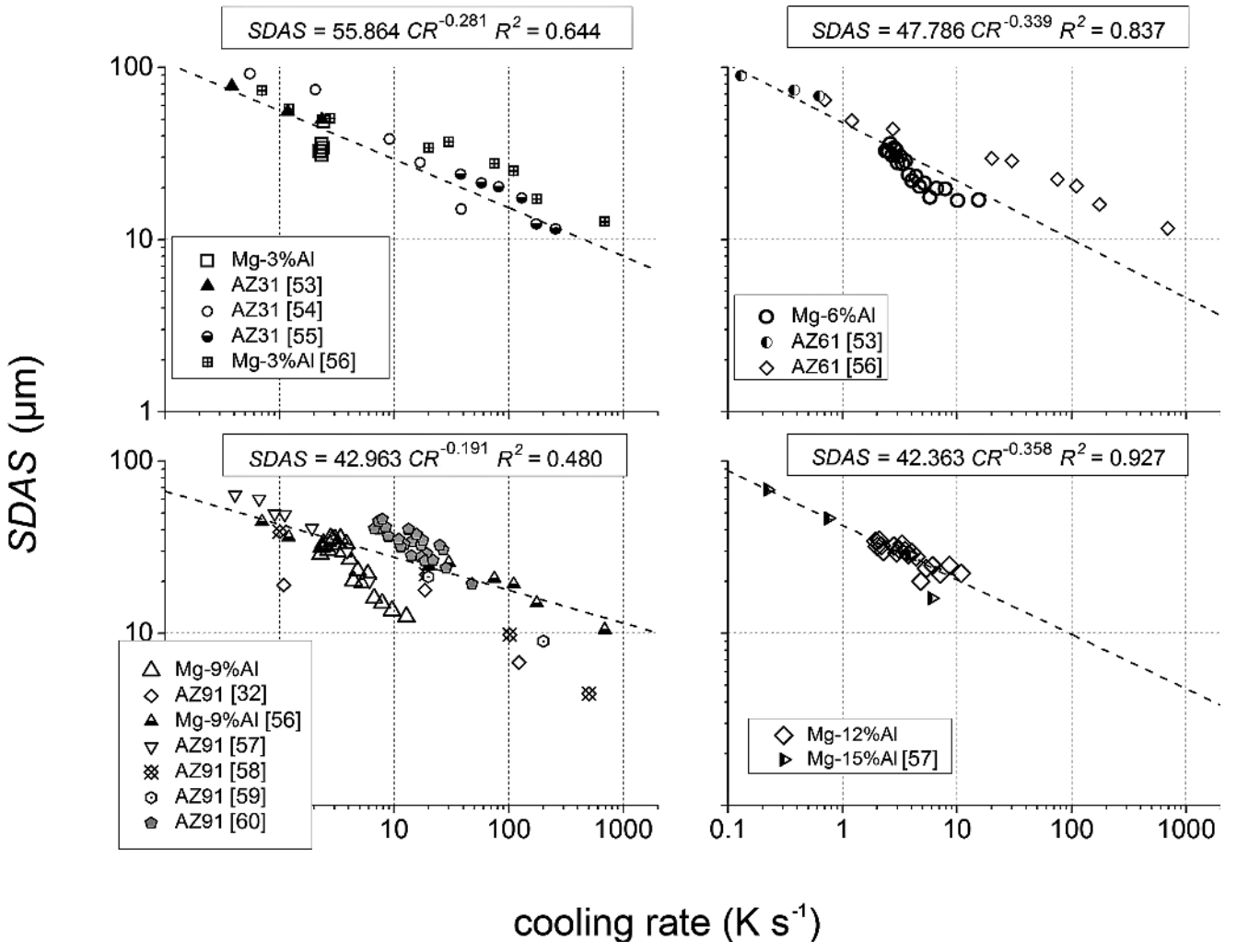

Fig. 15. Double logarithmic presentation of *SDAS* as a function of the cooling rate. Comparison to literature Refs. [32, 53–60].

mined from Eq. (3) through linear regression from the logarithmic presentation. The data for the adjusted line from Fig. 15 [32, 53–60] are summarized in Table 2. It shows that the progression of *SDAS* as a function of the cooling rate is similar for all aluminum contents. This applies at least to aluminum contents between 6 and 12 %. For the magnesium alloy with a 3 % Al content, not enough data are present to explicitly determine whether these *SDAS* are also independent of Al content. In Tables 3 and 4, the results of the structural examinations are summed and the effects on the corrosion behavior are postulated.

5. Conclusions

The structures of magnesium–aluminum alloys with 0, 3, 6, 9, and 12 % Al cast in a mold were examined with respect to different cooling rates (2 to 30 K s^{-1}). It was shown that an increased aluminum content increases grain fineness; however, an increased cooling rate had a bigger influence on the grain size and *SDAS*. The modeling of *SDAS* according to $\lambda_2 = K\left(M\frac{(T_L - T_E)}{CR}\right)^{1/3}$ revealed average K values between 4.3 and 8.3 and a gradient of around –1/3. A decrease in grain size with an increased cooling rate follows the *SDAS* with a similar gradient. The proportions of segregated β phase increase with aluminum content and cooling rate. The segregation in the form of dense β phase from the divorced eutectic and lamellar β phase from the saturated α phase are predominantly situated at the grain boundaries. With respect to changes in grain size, *SDAS*, and alignment and proportions of the β phase, an influence on the corrosion properties of the magnesium alloys is expected, which will be examined in part 2.

The authors thank the Deutsche Forschungsgemeinschaft for financial support of the project Di492/11–1 "Dendritic Structure Formation of Magnesium Alloys for the Manipulation of Corrosive Properties".

Table 2. Coefficients of the best-fit line from Fig. 15. Adjustment function for grain sizes and *SDAS* in the form of $y = A(CR)^B$.

Al (%)	Grain size (µm)		*SDAS* µm								
			From experiments			From theory $B = -1/3$			Experimental plus literature values from Fig. 15		
	A	*B*	*A*	*B*	*K*	*A*	*B*	*K*	*A*	*B*	*K*
3	423.87	–0.58	–	–	–	47.17		3.7	55.86	–0.28	6.5
6	165.44	–0.30	53.19	–0.53	1.6	41.55		4.6	47.79	–0.34	5.1
9	182.65	–0.45	57.70	–0.57	2.0	42.78	–0.33	6.0	42.96	–0.19	14.0
12	160.00	–0.36	40.58	–0.27	9.4	43.63		7.3	42.36	–0.36	7.7
mean value		–0.37		–0.46	4.3		–0.33	5.4		–0.29	8.3

Table 3. Influence of cooling rate on the structure of magnesium alloys with 3 to 12 % Al. The postulated corrosion rate is in brackets.

Cooling rate		high		low	
Grain size		small	(big)	big	(small)
SDAS		small	(big)	big	(small)
Enrichment Al in the α dendrites		big	(small)	small	(big)
Proportion of ß phase	Interdendritic	constant	(constant)	constant	(constant)
	Solid on grain boundaries	big	(big)	small	(small)

Table 4. Influence of aluminum content on the structure of magnesium alloys with 3 to 12 % Al. The postulated cooling rate is in brackets.

Aluminum content		high		low	
Grain size		small	(big)	big	(small)
SDAS		small	(big)	big	(small)
Enrichment Al in the α dendrites		big	(small)	small	(big)
Proportion of ß phase	Interdendritic	big	(big)	small	(small)
	Solid at grain boundaries	big	(big)	small	(small)
	lamellar	big	(big)	small	(small)

References

[1] C. Scharf, A. Ditze, A. Shkurankov, E. Morales, C. Blawert, W. Dietzel, K-U. Kainer: Adv. Eng. Mater. 7 (2005) 1134. DOI:10.1002/adem.200500180

[2] G. Song, A. Atrens, M. Dargusch: Corros. Sci. 41 (1998) 249. DOI:10.1016/S0010-938X(98)00121-8

[3] O. Lunder, J.H. Nordien, K. Nisancioglu: Corros. Rev. 15 (1997) 414. DOI:10.1515/CORRREV.1997.15.3-4.439

[4] Z. Shi, G. Song, A. Atrens: Corros. Sci. 47 (2005) 2760. DOI:10.1016/j.corsci.2004.11.004

[5] T. Zhang, Y. Li, F. Wang: Corros. Sci. 48 (2006) 1249. DOI:10.1016/j.corsci.2005.05.011

[6] R. Ambat, N.N. Aung, W. Zhou: Corros. Sci. 42 (2000) 1433. DOI:10.1016/S0010-938X(99)00143-2

[7] S. Mathieu, C. Rapin, J. Steinmetz, P. Steinmetz: Corros. Sci. 45 (2003) 2741. DOI:10.1016/S0010-938X(03)00109-4

[8] M. Jönsson, D. Persson, C. Leygraf: Corros. Sci. 50 (2008) 1406. DOI:10.1016/j.corsci.2007.12.005

[9] T. Abu Leil, N. Hort, W. Dietzel, C. Blawert, Y. Huang, K.U. Kainer, K.P. Rao: Trans. Nonferrous Met. Soc. China 19 (2009) 40. DOI:10.1016/S1003-6326(08)60225-3

[10] S. Feliu, A. Pardo, M.C. Merino, A.E. Coy, F. Viejo, R. Arrabal: Appl. Surf. Sci. 255 (2009) 4102. DOI:10.1016/j.apsusc.2008.10.095

[11] A. Pardo, M.C. Merino, A.E. Coy, R. Arrabal, F. Viejo, E. Matykina: Corros. Sci. 50 (2008) 823. DOI:10.1016/j.corsci.2007.11.005

[12] S. Izumi, M. Yamasaki, Y. Kawamura: Corros. Sci. 51 (2009) 395. DOI:10.1016/j.corsci.2008.11.003

[13] W.C. Neil, M. Forsyth, P.C. Howlett, C.R. Hutchinson, B. Hinton: Corros. Sci. 51 (2009) 387. DOI:10.1016/j.corsci.2008.11.005

[14] J.-x. Niu, Q.-r. Chen, N.-x. Xu, Z.-l Wei: Trans. Nonferrous Met. Soc. China 18 (2008) 1058. DOI:10.1016/S1003-6326(08)60181-8N

[15] Y. Fan, G. Wu, C. Zhai: Mater. Sci. Eng. A 433 (2006) 208. DOI:10.1016/j.msea.2006.06.109

[16] A. Pardo, M.C. Merino, A.E. Coy, F. Viejo, R. Arrabal, S. Feliú: Electrochim. Acta 53 (2008) 7890. DOI:10.1016/j.electacta.2008.06.001

[17] Y. Fan, G. Wu, H. Gao, G. Li, C. Zhai: J. Mater. Sci 41 (2006) 5409. DOI:10.1007/s10853-006-0256-8

[18] M.-C. Zhao, M. Liu, G. Song, A. Atrens: Corros. Sci. 50 (2008) 1939. DOI:10.1016/j.corsci.2008.04.010

[19] S. Amira, D. Dubé, R. Tremblay, E. Ghali: Mater. Charact. 59 (2008) 1508. DOI:10.1016/j.matchar.2008.01.018

[20] M.-C. Zhao, M. Liu, G. Song, A. Atrens: Adv. Eng. Mater. 10 (2008) 104. DOI:10.1002/adem.200700246

[21] G. Ben-Hamu, D. Eliezer, A. Kaya, Y.G. Na, K.S. Shin: Mater. Sci. Eng. A 435–436 (2006) 579. DOI:10.1016/j.msea.2006.07.109

[22] E. Zhang, W. He, H. Du, K. Yang: Mater. Sci. Eng. A 488 (2008) 102. DOI:10.1016/j.msea.2007.10.056

[23] N. Birbilis, M.A. Easton, A.D. Sudholz, S.M. Zhu, M.A Gibson: Corros. Sci. 51 (2009) 683. DOI:10.1016/j.corsci.2008.12.012

[24] G. Wu, Y. Fan, H. Gao, C. Zhai, Y.P. Zhu: Mater. Sci. Eng. A 408 (2005) 255. DOI:10.1016/j.msea.2005.08.011

[25] M. Jönsson, D. Thierry, N. LeBozec: Corrosi. Sci. 48 (2006) 1193. DOI:10.1016/j.corsci.2005.05.008

[26] R.K. Singh Raman: Metall. Mater. Trans. A 35 (2004) 2525. DOI:10.1007/s11661-006-0233-5

[27] M. Jönsson, D. Persson, R. Gubner: J. Electrochem. Soc. 154 (2007) C684. DOI:10.1149/1.2779957

[28] C. op't Hoog, N. Birbilis, Y. Estrin: Adv. Eng. Mater. 10 (2008) 579. DOI:10.1002/adem.200800046

[29] G. Song, A.L. Bowles, D.H. StJohn: Mater. Sci. Eng. A 366 (2004) 74. DOI:10.1016/j.msea.2003.08.060

[30] Y. Liu, D. Liu, C. You, M. Chen: Front. Mater. Sci. 9 (2015) 247. DOI:10.1007/s11706-015-0299-3

[31] P. Donelan: Mater. Sci. Tech. 16 (2013) 261. DOI:10.1179/026708300101507811

[32] D. Dubé, A. Couture, Y. Carbonneau, M. Fiset, R. Angers, R. Tremblay: Int. J. Cast Metal. Res. 11 (1998) 139. DOI:10.1080/13640461.1998.11819268

[33] J.M.V. Quaresma, C.A. Santos, A. Garcia: Metall. Mater. Trans. A 31 (2000) 3167. DOI:10.1007/s11661-000-0096-0

[34] W.R. Osório, A. Garcia: Mater. Sci. Eng. A 325 (2002) 103. DOI:10.1016/S0921-5093(01)01455-1

[35] W.R. Osório, C.A. Santos, J. Quaresma, A. Garcia: J. Mater. Process. Tech. 143–144, 703–709 (2003). DOI:10.1016/S0924-0136(03)00355-8

[36] M. Yang, S.-M. Xiong, Z. GuO: Acta Mater. 112 (2016) 261. DOI:10.1016/j.actamat.2016.04.014

[37] J. Du, Z. GuO, M. Yang, S.-M. Xiong: Mater. Today Comm. 13 (2017) 155. DOI:10.1016/j.mtcomm.2017.09.009

[38] J. Du, Z. GuO, A. Zhang, M. Yang, M. Li, S.-M. Xiong: Sci. Rep. 7 : 13600 (2017) 1. DOI:10.1038/s41598-017-12814-5

[39] J. Du, A. Zhang, Z. GuO, M. Yang, M. Li, S.-M. Xiong: ACS Omega 2 (2017) 8803. DOI:10.1021/acsomega.7b01174

[40] D. Bouchard, J.S. Kirkaldy: Metall. Mater. Trans. B 28 (1997) 651. DOI:10.1007/s11663-997-0039-x

[41] D.H. Kirkwood: Mater. Sci. Eng. 73 (1985) L1. DOI:10.1016/0025-5416(85)90319-2

[42] W. Kurz, D.J. Fisher: Fundamentals of Solidification, Switzerland, Trans Tech Public; (1986) 216. DOI:10.1002/crat.2170210909

[43] R. Trivedi: Metall. Trans. A 15 (1984) 977. DOI:10.1007/BF02644689

[44] A. Ditze, C. Scharf: Recycling of Magnesium, Papierflieger Verlag, Clausthal-Zellerfeld (2008) 76.

[45] K.P. Young, D.H. Kerkwood: Metall. Trans. A 6 (1975) 197. DOI:10.1007/BF02673688

[46] T.F. Bower, H.D. Brody, M.C. Flemings: Trans. TMS-AIME No 236 (1966) 624.

[47] T.Z Kattamis, J. Coughlin, M.C. Flemings: Trans. TMS-AIME No 239 (1967) 1504.

[48] A.B. Michael, M.B. Bever: Trans. TMS-AIME No 200 (1954) 47.

[49] J. Horwath, L. Mondolfo: Acta Metall. 10 (1962) 1037. DOI:10.1016/0001-6160(62)90072-X

[50] T. Okamoto, K. Kishitake: J. Cryst. Growth 29 (1975) 137. DOI:10.1016/0022-0248(75)90217-1

[51] M.A. Taha: Met. Sci. 13 (1979) 9. DOI:10.1179/030634579790434187

[52] R. Günther, C. Hartig, R. Bormann: Acta Mater. 54 (2006) 5591. DOI:10.1016/j.actamat.2006.07.035

[53] M. Paliwal, D.H. Kang, E. Essadiqi, I. Jung: Metall. Mater. Trans. A 45 (2014) 3596. DOI:10.1007/s11661-014-2288-z

[54] M. Masoumi, M. Pekguleryuz: AFS Trans. 117 (2009) 617.

[55] Y. He, A. Javaid, E. Essadiqi, M. Shehata: Can. Metall. Quart. 48 (2009) 145. DOI:10.1179/cmq.2009.48.2.145

[56] M. Paliwal, I.H. Jung: Acta Mater. 61 (2013) 4848. DOI:10.1016/j.actamat.2013.04.063

[57] C.H. Cáceres, C.J. Davidson, J.R. Griffiths, C.L. Newton: Mater. Sci. Eng. A 325 (2002) 344. DOI:10.1016/S0921-5093(01)01467-8

[58] H. Yin, S.D. Felicelli: Mater. Sci. Eng. 17 (2009)1. DOI:10.1088/0965-0393/17/7/075011

[59] W.P. Sequeira, M.T. Murray, G.L. Dunlop, D.H. StJohn, in: Proc. Symposium on automotive alloys, Orlando, Florida, TMS (1997) 169.

[60] C. Do Lee, K.S. Shin: Met. Mater. Int. 9 (2003) 21. DOI:10.1007/BF03027225

[61] U. Feurer, R. Wunderlin: Einfluss der Zusammensetzung und der Erstarrungsbedingungen auf die Dendritenmorphologie binärer Aluminiumlegierungen, Oberursel: Deutsche Gesellschaft für Metallkunde (1977) 8.

[62] D. StJohn, H. David, M. Qian, M.A. Easton, P. Cao, Z. Hildebrand: Metall. Mater. Trans. A 36 (2005) 1669. DOI:10.1007/s11661-005-0030-6

[63] S. Khan, N. Hort, E. Subasic, S. Schmauder: 10th Asian Foundry Congress, AFC-10, 21.–24.05.2008 (2008).
[64] W. Cao, S.-L. Chen, F. Zhang, K. Wu, Y. Yang, Y.A. Chang, R. Schmid-Fetzer, W.A. Oates: Calphad 33 (2009) 328. DOI:10.1016/j.calphad.2008.08.004

(Received March 23, 2018; accepted June 28, 2018; online since October 2, 2018)

Correspondence address

André Ditze
Engineering Office MetuRec
An den Eschenbacher Teichen 16
38678 Clausthal-Zellerfeld
Germany
Tel.: 0049 170 839 1069
E-mail: andre.ditze@t-online.de
Web: www.meturec.de

Bibliography
DOI 10.3139/146.111708
Int. J. Mater. Res. (formerly Z. Metallkd.)
109 (2018) 12; page 1081–1091

ISSN 1862-5282